# STATE-OF-THE-ART REVIEW OF COMPUTATIONAL FLUID DYNAMICS MODELING FOR FLUID-SOLIDS SYSTEMS

by

Robert W. Lyczkowski, Jacques X. Bouillard, Jainmin Ding+, Shen-Lin Chang, and Steven Lottes
**ARGONNE NATIONAL LABORATORY**
Energy Systems Division
+Energy Technology Division
9700 South Cass Avenue
Argonne, IL 60439-4815 USA

and

Steve W. Burge
**BABCOCK & WILCOX**
Alliance Research Center
1662 Beeson Street
Alliance, OH 44601-2196



Manuscript for an Invited Paper Submitted to
International Symposium on Parallel Computing
in Multiphase Flow Systems Simulations
1994 Winter Annual Meeting
American Society of Mechanical Engineers
November 6-11, 1994
Chicago, Illinois



May 12, 1994

# STATE-OF-THE-ART REVIEW OF COMPUTATIONAL FLUID DYNAMICS MODELING FOR FLUID-SOLIDS SYSTEMS*

**Robert W. Lyczkowski, Jacques X. Bouillard, Jianmin Ding+, Shen-Lin Chang, and Steven Lottes**
Energy Systems Division
Argonne National Laboratory
Argonne, Illinois

**Steve W. Burge**
Babcock & Wilcox
Alliance Research Center
Alliance, Ohio

## ABSTRACT

As the result of 15 years of research (50 staff years of effort) Argonne National Laboratory (ANL), through its involvement in fluidized-bed combustion, magnetohydrodynamics, and a variety of environmental programs, has produced extensive computational fluid dynamics (CFD) software and models to predict the multiphase hydrodynamic and reactive behavior of fluid-solids motions and interactions in complex fluidized-bed reactors (FBRs) and slurry systems. This has resulted in the FLUFIX, IRF, and SLUFIX computer programs.

These programs are based on fluid-solids hydrodynamic models and can predict information important to the designer of atmospheric or pressurized bubbling and circulating FBR, fluid catalytic cracking (FCC) and slurry units to guarantee optimum efficiency with minimum release of pollutants into the environment. This latter issue will become of paramount importance with the enactment of the Clean Air Act Amendment (CAAA) of 1995. Solids motion is also the key to understanding erosion processes. Erosion rates in FBRs and pneumatic and slurry components are computed by ANL's EROSION code to predict the potential metal wastage of FBR walls, internals, feed distributors, and cyclones.

Only the FLUFIX and IRF codes will be reviewed in the paper together with highlights of the validations because of length limitations. It is envisioned that one day, these codes with user-friendly pre- and post-processor software and tailored for massively parallel multiprocessor shared memory computational platforms will be used by industry and researchers to assist in reducing and/or eliminating the environmental and economic barriers which limit full consideration of coal, shale and biomass as energy sources, to retain energy security, and to remediate waste and ecological problems.

## NOMENCLATURE

| | |
|---|---|
| a,b | Transport coefficients (see Eq. 15) |
| $C_d$ | Drag coefficient (see Eq. 8) |
| c | Compaction modulus |
| $d_p$ | Particle diameter, m |
| g | Acceleration due to gravity in the x, y, and z-directions, = $g_x$,$g_y$,$g_z$, m/s$^2$ |
| $G_k$ | Solids elastic modulus for phase k ($G_f = 0$), Pa |
| $\bar{\bar{I}}$ | Unity tensor |
| L | Characteristic length or mean free path, m |
| $\overline{M}$ | Molecular weight, kg/mol |
| $\dot{m}_k$ | Mass source for phase k, kg/(m$^3$·s) |
| p | Pressure, Pa |
| $\overline{R}$ | Universal gas constant in the ideal gas law, J/(mol·K) |
| $R_i$ | Flow resistance coefficients for flow in the x-, y-, and z-directions, = $R_x$, $R_y$,$R_z$, m$^{-1}$ |
| Re | Reynolds Number |
| S | Source term |
| $v_k$ | Velocity of phase k, m/s |

+Present Address:
Energy Technology Division
Argonne National Laboratory
Argonne, Illinois

* Work supported by U.S. Department of Energy, Assistant Secretary for Fossil Energy, under Contract W-31-109-ENG-38.

### Greek Letters

| | |
|---|---|
| $\beta_A, \beta_B$, | Fluid-particle friction (drag) coefficients for hydrodynamic models A and B, respectively, kg/(m$^3$·s) |
| $\gamma_v$ | Volume porosity |
| $\gamma_i$ | Surface permeabilities in the x-, y-, and z-directions, $= \gamma_x, \gamma_y, \gamma_z$ |
| $\varepsilon_k$ | Volume fraction of phase k, $\varepsilon_f = 1 - \varepsilon_s$, $\varepsilon_f = \varepsilon$ |
| $\varepsilon^*$ | Compaction gas volume fraction |
| $\zeta_k$ | A parameter used to select the hydrodynamic model for phase k |
| $\kappa_k$ | Bulk viscosity of phase k, Pa·s |
| $\mu_k$ | Microscopic viscosity of phase k, Pa·s |
| $\rho_k$ | Microscopic density of phase k, kg/m$^3$ |
| $\rho'_k$ | Macroscopic density of phase k, $= \varepsilon_k \rho_k$, |
| $\bar{\bar{\tau}}_k$ | Viscous stress of phase k, Pa |
| $\phi$ | Dependent solution variable (see Eq. 15) or sphericity (also called shape factor) of solids |
| $\psi$ | Dependent solution variable (see Eq. 15) |

### Subscripts

| | |
|---|---|
| A | Hydrodynamic model A |
| B | Control volume in back of volume P or hydrodynamic model B |
| E | Control volume east of volume P |
| F | Control volume in front of volume P |
| N | Control volume north of volume P |
| P | Control volume of interest |
| Q | Subscript used to denote quantities at the center of main control volumes (see Eq. 15) |
| S | Control volume south of volume P |
| W | Control volume west of volume P |
| b | Back face |
| e | East face |
| f | Fluid phase or front face |
| i,k | Phase i or k (i = f,g, k = f,g) |
| p | Particle |
| q | Subscript used to denote quantities on the faces of a main or momentum control volume (see Eq. 15) |
| s | Solids phase or south face |
| w | west face |

### Operators

| | |
|---|---|
| $\nabla \cdot$ | Divergence |
| $\nabla$ | Gradient |

## 1. INTRODUCTION

Solids motion (and the associated bed dynamics involving bubble evolution and pressure fluctuations) is the key to understanding the transport processes in fluidized-bed reactors (FBRs). Fluidized-bed reactors are used industrially, but scale-up and erosion of in-bed tubes and other components is still hampering the commercialization of the FBR technology. Despite its importance, the exact mechanisms of scale-up and erosion in fluidized beds are poorly understood. Many models have been proposed for studying hydrodynamic phenomena in fluidized-bed reactors. Most of them are one- or two-dimensional models. The one-dimensional models, which include chemical reaction and pollutant formulation, rely heavily on simplifying assumptions.

Over the last 15 years, two- and three-dimensional models for gas-solids flow have been developed with a constant microscopic solids viscosity at IIT (Illinois Institute of Technology) (Gidaspow, 1986; Gidaspow and Ding, 1990) and at B & W (Babcock & Wilcox) (Burge, 1991) and with a kinetic theory model for hydrodynamics and erosion at ANL (Argonne National Laboratory) (Ding and Lyczkowski, 1992). Application of these models to studying gas-solids fluidization phenomena has been successfully carried out. Comparisons between computed results and experimental data have shown the significance of and necessity for three-dimensional models of hydrodynamics and erosion in bubbling fluidized beds (Ding and Lyczkowski, 1992). To date, no other published three-dimensional two-phase flow models have been used to simulate fluidized beds, to our knowledge. One reason has been extensive computing run time.

FLUFIX (Lyczkowski and Bouillard, 1992), ANL's flagship code, incorporated into the FORCE2 (Burge, 1991) computer code, is a two- or three-dimensional transient Eulerian finite-difference and finite-control-volume fluid flow and heat and mass transfer solver for gas-solids systems written in Cartesian and cylindrical coordinates. FLUFIX, like all our codes, is written in a modular form and uses the implicit multifield (IMF) numerical technique of Harlow and Amsden (1975). Computed are solids loading, gas and solids velocities, pressure, and temperatures. Applications are bubbling and circulating atmospheric and pressurized fluidized bed reactors, i.e. combustors, gasifiers, and FCC reactors. Predicted are bubble formation, bed frequencies, and solids recirculation.

SLUFIX (Lyczkowski and Wang, 1992) is a two- or three-dimensional, Eulerian, finite-difference and finite-control-volume fluid flow and heat and mass transfer solver for Newtonian and non-Newtonian liquid-solids systems. Applications are slurry transport and atomization and liquefaction reactors. Predicted are solids loadings, liquid and solids velocities, pressure, mixture viscosity and shear rate, and temperature.

EROSION (Lyczkowski et al., 1990, 1992) is a two- and three-dimensional finite-difference solver used to predict erosion rates of components in contact with fluid-solids systems. It incorporates Finnie's, Neilson-Gilchrist's and ANL's monolayer energy dissipation erosion models. Predicted are lifetimes of heat exchanger tubes, waterwall surfaces, internals, distributors, and baffles. Recommended is the use of FLUFIX or SLUFIX for inputs.

The FLUFIX and EROSION codes were extensively developed during a four year cooperative R&D venture, "Erosion of FBC Heat Transfer Tubes." Industrial participants in the R&D venture were ABB Combustion Engineering, Babcock & Wilcox, U.S. Department of Energy (DOE) Morgantown Energy Technology Center, Electric Power Research Institute, Foster Wheeler Development Corp., State of Illinois Center for Research in Coal, ASEA Babcock PFBC (now dissolved), and Tennessee Valley Authority. Late joining members added were British Coal Corporation (UK) and CISE (Milan, Italy).

A number of variants of the FLUFIX pilot code have been developed which address gas-solids and wall-solids/wall-gas heat transfer, multiple solids phases, multiple gas species chemically reactive flows, liquid-solids and gas-solids electrodynamics and magnetics, kinetic theory of granular flow, and three-phase, gas/liquid/solids. Further development of the codes continues and will incorporate boundary-fitted coordinates and finite element methods.

A multiphase reacting flow computer code developed by a team of Argonne National Laboratory (ANL) and University of Illinois at Chicago is capable of predicting flow characteristics and combustion processes in a reacting flow for a number of gaseous species and particles/droplets of various sizes. One unique feature of the computer code is an integral reaction submodel which provides the integral reacting flow (IRF) computer code much improved numerical stability and convergence behavior in combustion calculations (Chang and Lottes, 1993). The computer code has been used in various engineering applications including coal-fired combustors for magnetohydrodynamic (MHD) power generation (Lottes and Chang, 1992), air-breathing jet engines (Zhou and Chiu, 1983), and diesel engines (Chang and Wang, 1987), and validated partially by comparing calculations with experimental measurements. In this paper, discussion will focus on the simulation of a multiphase reacting flow in an MHD combustor.

Coal-fired MHD power generation which deals with an electrically conducting flow in the presence of a magnetic field can attain higher overall efficiency and produce less pollutants compared to a conventional power plant. The U.S. Department of Energy has been sponsoring a proof-of-concept program toward the commercialization of MHD power generation since early 1980. As a part of the team in the program, ANL used the integral reacting flow (IRF) computer code to investigate the multiphase flow characteristics in a prototypical 50 MWt MHD power train system (Chang et al., 1993). Among the most important considerations for the MHD technology are the attainment of high temperature from multi-stage coal-fired combustion and of high electric conductivity by injecting a seed material, i.e., potassium, into the combustion flow. ANL's computer simulation was found useful in resolving some critical technical issues in the development of the MHD technology, such as oxygen jet penetration, combustion efficiency, seed particle evaporation, seed vapor mixing, and particle wall deposition.

Extensive validation of ANL's multiphase, hydrodynamic, and reactive fluid-solids flow codes and models has been made over the past 15 years; this is one of ANL's particular strengths in the area of reactive fluids-solid flow analyses. State-of-the-art multiphase laser velocimetry, gammametry, nuclear magnetic resonance (NMR) and ultra sound tomographic imaging techniques have been used to develop the data used in validation and calibration. Some of these validations are discussed in this paper for the FLUFIX and IRF codes.

All of the above codes have been developed for CRAY supercomputers, IBM mainframe computers, VAX minicomputers, personal computers, and high-end workstations, such as IBM RISC, SUN, and Silicon Graphics. These computational fluid dynamic softwares are also being upgraded to utilize massively parallel processors, such as the ANL IBM SP-1, and multigrid convergence acceleration techniques. In this paper, a proposed strategy for this effort is briefly discussed.

Argonne National Laboratory continues to work with industry in applying these computer programs to a broad spectrum of problems. The FLUFIX and EROSION codes have been used extensively to study hydrodynamics and erosion in atmospheric and pressurized bubbling (dense) and circulating (turbulent) fluidized bed combustors, e.g. British Coal Corporation, Babcock & Wilcox R&D, ABB Combustion Engineering, and Ahlstrom Pyropower, Inc. Currently, discussions are underway with a number of organizations to utilize the codes to analyze FCC and FBC reactors, e.g. UOP, Chevron Research & Technology, Dow Corning Corporation, and E.I. du Pont de Nemours & Co., Inc.

## 2. FLUFIX HYDRODYNAMIC MODELS

The hydrodynamic approach to fluidization which was started by Davidson (1961) is the basis for the models implemented in FLUFIX, which is incorporated into FORCE2. All the solid particles having identical densities and diameters form a continuum. The fluid and solids phases are then treated as interpenetrating fluids in an Eulerian formulation. Conservation of mass and momentum are then applied to each phase (a total of two or more) to derive the hydrodynamic model. Both single and multiple particle phases have been simulated with this approach (Gidaspow, 1986). The current FORCE2 model considers only two phases: one fluid phase, which can be a gas or liquid and one solids phase. The capabilities of several computer codes utilizing this approach were reviewed by Smoot (1984) and Gidaspow (1986). Work at ANL using the FLUFIX/MOD2 computer code (Lyczkowski and Bouillard, 1992) to model IIT's small-scale thin "two-dimensional" fluidized bed has provided partial validation of the hydrodynamic model.

Two hydrodynamic models, called Models A and B by Lyczkowski and Bouillard (1992) have been implemented in FORCE2. They are extensions of the models developed by Lyczkowski et al. (1990, 1992) for the FLUFIX code. The models have been extended in FORCE2 to include: (1) three-dimensional Cartesian and cylindrical geometry; (2) volume porosities and surface permeabilities to account for volume and surface obstructions in the flow field, and (3) distributed resistance to account for pressure drops caused by baffles, distributor plates, and large tube bundles. The hydrodynamic models of fluidization uses the principles of conservation of mass, momentum, and energy. The continuity equations and the separated phase momentum equations for three-dimensional, transient, and isothermal two-phase flow are given below.

Continuity equations

$$\frac{\partial}{\partial t}(\rho'_k\gamma_v) + \nabla \cdot (\rho'_k\gamma_i v_k) = \gamma_v \dot{m}_k \tag{1}$$

where $\rho'_k = \varepsilon_k\rho_k$ is the macroscopic density, the subscript k denotes the phase (i.e., k = f for the fluid phase and k = s for the solids phase), $\varepsilon_k$ is the phase volume fraction, $\gamma_i$ are the surface permeabilities, $\gamma_v$ is the volume porosity, and $v_k$ is the phase velocity vector.

Momentum equations

$$\frac{\partial}{\partial t}(\rho'_k\gamma_v v_k) + \nabla \cdot (\rho'_k\gamma_i v_k v_k) = -\zeta_k\gamma_v\varepsilon_k\nabla p + \gamma_v\rho'_k g - \gamma_v R_i \frac{\rho'_k v_k^2}{2} - \gamma_v\beta_M (v_i - v_k) + \gamma_v G_k \nabla\varepsilon_g + \nabla\cdot\bar{\bar{\tau}}_k \tag{2}$$

where

$$\bar{\bar{\tau}}_k = \varepsilon_k\mu_k\gamma_i\left[\nabla v_k + (\nabla v_k{}^T)\right] - \gamma_i\varepsilon_k\lambda_k(\nabla\cdot v_k)\bar{\bar{I}}, \tag{3}$$

and

$$\lambda_k = \frac{2}{3}\mu_k - \kappa_k \tag{4}$$

$\kappa_k$ is the bulk viscosity for phase k. The parameter, $\zeta_k$, is used to select the hydrodynamic model according to model A or model B. For model A, $\zeta_{f,s} = 1$ for both the fluid and the solids phase. For model B, $\zeta_f = 1/\varepsilon$ and $\zeta_s = 0$, where $\varepsilon = \varepsilon_f$.

Standard correlations are used to evaluate the fluid-particle friction (drag). However, the drag coefficients $\beta_M$ (M = A or B) depend on the model selected. According to Lyczkowski and Bouillard (1992), the relation between $\beta_A$ and $\beta_B$ is

$$\beta_B = \beta_A/\varepsilon \tag{5}$$

$\beta_A$ is obtained from the Ergun equation (Ergun, 1952) for $\varepsilon \le 0.8$ and from Wen and Yu's (1966) correlation for $\varepsilon > 0.8$. These expressions may be summarized as follows:

For $\varepsilon \le 0.8$,

$$\beta_A = 150\frac{\varepsilon_s^2\mu_f}{\varepsilon(d_p\phi_s)^2} + 1.75\frac{\rho_g\varepsilon_s|v_f - v_s|}{d_p\phi_s} \tag{6}$$

For $\varepsilon > 0.8$,

$$\beta_A = \frac{3}{4}C_d\frac{\varepsilon\varepsilon_s\rho_f|v_f - v_s|}{d_p\phi_s}\varepsilon^{-2.7} \tag{7}$$

where

$$C_d = \frac{24}{Re_p}\left[1 + 0.15Re_p^{0.687}\right], \text{ for } Re_p \le 1000 \tag{8}$$

$$C_d = 0.44, \text{ for } Re_p > 1000, \tag{9}$$

$$Re_p = \frac{\varepsilon\rho_g|v_f - v_s|d_p\phi_s}{\mu_f} \tag{10}$$

The particle sphericity (also called shape factor), $\phi_s$, is defined as the ratio of the actual surface area of the particle to the surface area of a spherical particle of diameter $d_p$.

The solids elastic modules, $G_s$, is used to calculate the normal component of the solids stress through the relation $G_s\nabla\varepsilon$. The primary computational function of the solids stress term is to keep the bed from compacting below the defluidized of packed bed state. Any solids stress model that accomplishes this is adequate. Here we use

$$G_s = G_0\exp\left[-c(\varepsilon - \varepsilon^*)\right] \tag{11}$$

as discussed by Lyczkowski and Bouillard (1992). In this paper we use c = 600, $\varepsilon^* = 0.376$ used by Lyczkowski and Bouillard (1992). c = 500, $\varepsilon^* = 0.422$ were used by Gidaspow and Syamlal (1985). $G_0$ has been taken as 1.0 Pa.

The three resistance coefficients, $R_i$, i = x,y,z, are input to the models and can be replaced with correlations.

The gas density is determined by the ideal gas law,

$$\rho_g = \frac{\bar{M}p}{\bar{R}T} \tag{12}$$

where $\bar{M}$ is the average molecular weight, T is the absolute temperature, and $\bar{R}$ is the universal gas constant. For the fluid phase, the solids elastic modulus, $G_f$, is set to zero.

To solve the three-dimensional equations of fluid-solids flow given above, we need appropriate initial conditions and boundary conditions for the two phase velocities, the fluid phase pressure, and the porosity. The initial conditions depend upon the problem investigated. The inlet conditions are usually given. For example, the porosity is set to 1 where particle-free fluid enters the system. The boundary conditions at planes of symmetry demand zero normal gradient of all variables.

At an impenetrable solid wall, the fluid phase velocities in the three normal and tangential directions are set to zero. The no-slip condition cannot always be applied to the solids phase. Since the particle diameter is usually larger than the length scale of surface roughness of the rigid wall, the

particles may partially slip at the wall. This mean slip velocity is given by

$$v_s|_w = -L\frac{\partial v_s}{\partial \xi}\Big|_w \qquad (13)$$

where the $\xi$ direction is normal to the wall. The slip parameter, L, is taken to be the mean distance between particles. In FORCE2 and FLUFIX/MOD2, the mean free path is determined by

$$L = d_p\phi_s/(6\sqrt{2}\varepsilon_s) \qquad (14)$$

Also the mean free path can be derived directly from kinetic theory of granular flow (Ding and Lyczkowski, 1992).

## 3. FORCE2 CODE SUMMARY

The partial differential equations with appropriate initial and boundary conditions described in the preceding section are solved by FORCE2 using the finite-difference method. The finite-difference equations are derived by dividing the flow domain into a collection of control volumes and then integrating the governing momentum and continuity equations over these volumes. This results in a set of coupled, non-linear equations describing the velocities, void fractions, and pressures within the volumes.

The flow (or computational) domain is divided into a collection of cells or control volumes in a Cartesian coordinate system. Scalar quantities such as pressure and void fraction are calculated at the centers of these volumes denoted Main Control Volumes. Fluid and solids velocities are calculated on the Main Volume faces utilizing a second set of control volumes that are "staggered" with respect to the Main Volumes. This second set of volumes connect the centers of the Main Volumes and are called Momentum Control Volumes. The collection of Main and Momentum Volumes is the conventional "staggered" mesh used in most finite-difference formulations (Patankar, 1980). A general finite-difference transport equation (representing conservation of mass or momentum) may then be derived using the general control volume arrangement as

$$a_p\phi_P = \sum a_q\phi_Q + b_p\psi_P + S_c \qquad (15)$$

where $\phi_P$ and $\psi_P$ are dependent solution variables, $a_q$ is the transport coefficients on face q of control volume P, $\sum a_q\phi_Q = a_e\phi_E + a_w\phi_W + a_n\phi_N + a_s\phi_S + a_f\phi_F + a_b\phi_B$, $a_p = \sum a_q + b_p + S_P$, $S_c$ is a source of $\phi_P$, $S_P$ is a positive coefficient for a source of $\phi_P$, and $b_p$ is a positive coefficient linking the two dependent variables $\phi_P$ and $\psi_P$. Details about this equation can be found in Patankar's book (1980) or the FORCE2 documentation (Burge, 1991).

For transient simulations, the implicit multifield (IMF) technique (Harlow and Amsden, 1975) is used in FORCE2 and is based primarily on the IMF scheme as implemented in FLUFIX/MOD2. The solution procedure is based on adjusting the node pressure until fluid phase mass is conserved. Some key features of the method include: (1) cell-by-cell solution, (2) simultaneous solution for velocities on the cell faces, (3) explicit formulation for convection and diffusion, and (4) implicit formulation for solids stresses.

For steady-state simulations, because the finite-difference form of the momentum and continuity equations are very nonlinear, an iterative solution procedure is required. The approach is to construct sets of linear equations by evaluating the velocity, void fraction, etc., coefficients based on assumed or trial operating conditions. The resulting linear equations are solved using matrix methods and their solutions used to estimate new operating conditions. This sequence is continued until the equation residuals are small indicating that an acceptable solution has been achieved. The nonlinear nature of the governing equations also requires that the solution be advanced slowly. A key element of the solution scheme is the adjustment of the flow field pressure to conserve mass in each computational cell. The iterative procedure is based on conserving mass once a solution is achieved. The solution procedure is a modified version of SIMPLER (Patankar, 1980) developed by Schnipke (1986).

## 4. VALIDATION OF FORCE2

Validation of FORCE2 was identified as a key step in making the computer program a useful tool for industry and was, therefore, initiated as part the in-kind work for the Cooperative R&D Venture described in the Acknowledgments Section. Although FORCE2 is fundamentally based and, therefore, could be applied to both atmospheric and pressurized bubbling and circulating fluidized beds and liquid-solids fluidized beds and slurries, the current effort focused on validation for atmospheric bubbling gas-solids fluidized beds.

Three sources of data were selected to validate FORCE2. In the following simulations, the solids viscosity is assumed to be 0.1 Pa·s (1.0 poise) except when it is zero (inviscid solution).

### 4.1. FLUFIX and the FLUFIX Standard Problem

A standard problem has been formulated by ANL (Lyczkowski and Bouillard, 1992) from tests conducted at IIT (Bouillard et al., 1989) on a thin "two-dimensional" fluidized bed with an immersed obstacle located above an inlet air jet. This fluidized bed was $40 \times 3.81$ cm in cross-section with a central jet velocity of 5.78 m/s. The jet inlet width was 1.27 cm. A rectangular obstacle ($9.74 \times 2.54$ cm) was placed approximately 9.74 cm above the jet. The bed material was glass beads having a particle diameter of 500 μm and a density of $2.5 \times 10^3$ kg/m$^3$. The initial bed height was 29.9 cm. Time-averaged porosities were obtained using a Cs-137 gamma-ray source and detected with an ionization gauge.

The FORCE2 and FLUFIX/MOD2 grid structure were developed by assuming a symmetry plane through the central jet. As a result, only half of the bed is modeled. The FORCE2 nodal structure, which was identical to that used in FLUFIX/MOD2, is depicted in Fig. 1. The predicted gas void fractions from FLUFIX/MOD2 and FORCE2 and the measured time-averaged void fractions at 10 cm and 17 cm from the

center of the jet are respectively shown in Figs. 2 and 3. Instantaneous gas void fractions predicted by FLUFIX/MOD2 and FORCE in the node above the inlet jet are shown in Fig. 4. The predicted results of FORCE2 reasonably agree with the measured data and agree well with the predicted results of FLUFIX/MOD2. The agreement with the experimental data is promising and indicates that this fundamentally-based model does simulate the major hydrodynamic features of the bed.

### 4.2. CAPTF Three-Dimensional Fluidized Bed

A 30.5 × 30.5-cm square fluidized bed with two rows of tubes was tested in the Computer-Aided- Particle Tracking Facility (CAPTF) at the University of Illinois at Urbana-Champaign (UIUC) (Podolski et al., 1991). The bed material was glass beads with a mean particle diameter of 513 μm and a density of $2.5 \times 10^3$ kg/m$^3$. The initial bed height was 40.6 cm. Immersed tubes having an outer diameter of 5.08 cm were used. The bed was fluidized with a superficial air velocity of 52 cm/s. In FORCE2 model, the circular tubes were replaced by rectangular-shaped tubes, as depicted in Fig. 5.

The FORCE2 nodal structure used to simulate the bed is shown in Fig. 5. The bed is modeled in three dimensions with a total of approximately 1134 control volumes. The approximate locations of the pressure measurements (numbers 1-10 for the elevations and planes A, B, C) are also shown in Fig. 5. Figures 6 and 7 show the comparisons between measured and FORCE2 predicted power spectral densities of the pressure fluctuations located at A-10 and B-6, respectively. The frequencies of the maximum predicted power spectra at these locations approximately agree with the measured data. Neither the data nor FORCE2 indicate pronounced three-dimensional effects. The measured and predicted power spectrum at various elevations did not vary significantly from plane to plane (Burge, 1991). Based on these predictions, FORCE2 provided a reasonable simulation of the 3-D CAPTF tube bundle.

### 4.3. Foster Wheeler Half-Depth Tube Bundle

A series of pressure fluctuation and erosion tests were conducted by the Foster Wheeler Development Corporation (FWDC) on a two-row tube bundle in a bubbling fluidized bed (Podolski et al., 1991). Pressure fluctuation data collected during testing of the 76.2 cm deep (called the half-depth bundle) bed were used for the validation study here. The mean particle diameter was 1500 μm. The particle density was $1.28 \times 10^3$ kg/m$^3$. The initial bed height was 40.64 cm. The inlet air fluidizing velocity was 121.9 cm/s.

In the FORCE2 model, quarter-symmetry is assumed at the mid-width and mid-depth of the bed. The nodal structure is shown in Fig. 8. The computed pressure time series of 1100 points were used to determine the power spectral densities. Computed and measured power spectral of pressure fluctuations at locations A-2 and B-2 are shown in Figs. 9 and 10, respectively.

The predicted and the measured major frequencies compare favorably. Predicted and measured maximum powers occur in different planes, as shown in Fig. 11. This indicates the three-dimensional effects in the bed.

## 5. INTEGRAL REACTING FLOW (IRF) COMPUTER CODE MODELS AND SUMMARY

### 5.1. Formulation of the Code

The IRF code is for transient and steady-state analyses. Since MHD flow is a steady-state phenomenon, only the steady-state version of the code will be discussed here. The code employs the Eulerian approach for both gas and particle phases. General conservation laws, expressed by elliptic-type partial differential equations, are used in conjunction with rate equations governing the mass, momentum, enthalpy, species, turbulent kinetic energy, and turbulent dissipation for gaseous species and solid particles/droplets in a multiphase reacting flow. Some complex phenomena in the flow are modeled by simplified phenomenological submodels. These submodels include integral reaction, two-parameter turbulence, particle evaporation, and interfacial drag and heat transfer submodels. The integral reaction submodel converts rates of reaction heat release, consumption of fuel, and formation of products from reaction time scale to flow-time scale. The turbulence submodel is the standard k-ε model (Patankar, 1980), but modified to account for the effects of the solid phase. The evaporation submodel treats particle evaporation and size change over a spectrum of particle size. The interfacial submodel uses empirical correlations to calculate interfacial momentum and energy transfer.

The governing equations for gas species are the elliptic partial differential equations of fluid mechanics, including conservation of momentum, energy, and mass, with separate equations for chemical species conservation and turbulence. These equations contain source and sink terms for interphase exchange rates, the effect of reaction, etc. For convenience of numerical formulation the governing equations for gas phase are put in a common form:

$$\frac{\partial}{\partial x_i}\left(\theta\rho U_i\xi - \Gamma_\xi \frac{\partial \xi}{\partial x_i}\right) = S_\xi \qquad (16)$$

in which i is the dummy index indicating a summation from 1 to 2, θ is the gas phase volume fraction, Γ is the effective diffusivity, ξ is a general gas flow variable, representing a scalar, velocity components $U_1$ or $U_2$, fuel, inert, or seed vapor species $Y_{fu}$, $Y_{ir}$, or $Y_{sv}$, richness τ, enthalpy h, turbulent kinetic energy k, or turbulent dissipation rate ε. A richness equation which eliminates the source term in the transport equations to enhance numerical stability replaces the oxidizer species equation.

The solid phase transport equations include equations of particle number density (n), velocities ($U_{s,1}$, $U_{s,2}$), and temperature ($T_s$) for various particle sizes. For each particle size group, the convective and diffusive flux terms are

expressed as:

$$\frac{\partial}{\partial x_i}\left(nU_{s,i}\xi - \Gamma_\xi \frac{\partial n\xi}{\partial x_i}\right) = S_\xi. \qquad (17)$$

When $\xi = 1$, Eq. 17 is a number density equation; when $\xi = U_{s,1}$ or $U_{s,2}$, Eq. 17 is a particle momentum equation; and when $\xi = T_s$, Eq. 17 is a particle energy equation. The source term of the particle number density equation accounts for particle evaporation, while the diffusion term accounts for particle dispersion due to interaction with the turbulence of the gas phase. The interactions between phases are included in the source terms for both gas and particle phases. For example, a momentum sink in gas flow accounting for particle drag effects is also a momentum source for the solid flow.

Source terms and effective diffusion coefficients of the transport equations for both gas and solid phase flow variables are calculated using empirical correlations in submodels. For the source terms of the transport equations of fuel concentration and enthalpy, an integral reaction submodel is used to determine fuel consumption and heat release rates. For seed vapor concentration and particle number density, a particle evaporation submodel is used to determine particle evaporation and size dispersion rates. For gas and solid velocities, correlations of interfacial drag force are used to determine momentum exchanged between phases. For gas enthalpy and solid temperature, correlations of interfacial heat transfer are used to determine energy exchange between phases. For the effective diffusion coefficients of all transport equations, a submodel is used to determine turbulent diffusivity for both gas and solid phases

The governing non-linear partial differential equations, Eqs. 16 and 17, are solved numerically. A staggered grid system was used for the numerical calculation, with the gas velocity components stored on the cell surfaces and all other physical quantities stored at the nodal points of each cell (or scalar cell). The governing equations are transformed into algebraic equations by integrating over the computational cell which achieves conservation of flow properties independent of grid size. Patankar's (1980) SIMPLER numerical algorithm is modified to solve the discrete equations. These algebraic equations are solved using a line-by-line sweep in the primary flow direction to avoid numerical asymmetry. Particles are allowed to deposit on the walls by extrapolating the particle velocity to the walls. A momentum wall function is used to bridge the near wall boundary layer.

## 6. VALIDATION OF IRF

### 6.1. Numerical Convergence

The integral reacting flow computer code described above was used to simulate a reacting flow with vaporizing particles in an MHD combustor. The combustor was represented by a simple rectangular box consisting of four side walls with oxidizer injectors on two opposing walls and two openings for flow inlet and exit as shown in Fig. 12. Also in Fig. 12 is a two-dimensional grid defined on a cross-sectional area in the middle of the combustor away from the viscous effects near the front and back walls. The grid system consists of a horizontal x- (or $X_1$-) axis and a vertical y- (or $X_2$-) axis and its origin is set at the lower left corner. Evenly spaced grid points are defined for the y-axis and variably spaced grid points are defined for the x-axis. Dense grid points are selected near the jet opening where large flow property gradients are expected.

Determining the minimum amount of computational resources necessary to obtain good quality computational results with a relatively high confidence is a necessary step to control costs and allow a thorough parametric study to be done for a multiphase combustion flow simulation. A convergence and grid sensitivity study was conducted for MHD flow calculations to identify convergence levels for both gas and particle phases in which computed variables have converged to four or more decimal digits, to identify a level of grid refinement in which computed variables change little upon further grid refinement, and to identify a number of particle size groups in which computed particle variables change little upon further refinement of particle size space. Results of the sensitivity study indicate that if the average local mass residual is 9 orders of magnitude smaller than the inlet flow rate (or a convergence level of 9), the combustion calculation has converged to a minimum of four decimal digits over all of the grid points for all major variables. All calculations in the following discussion achieve the convergence level of 9 or above. Furthermore, the sensitivity study shows that a 54 by 32 grid and 5 particle size groups are required to obtain a convergent solution for a combusting flow with particle evaporation in the MHD combustor. Such a calculation takes about 2000 CPU seconds on a CRAY/XMP supercomputer.

### 6.2. Comparison of IRF with Measurements

Parametric studies were performed to investigate the effect of seed particle size and oxidizer injection angle on combustion efficiency, particle wall deposition, seed particle evaporation rate, and seed vapor distribution in the combustor. Common flow properties used in the parametric calculations are listed in Table I.

TABLE I COMMON FLOW PROPERTIES IN AN MHD COMBUSTOR

| | |
|---|---|
| Pressure (atm) = | 5.7 |
| Inlet Gas Temperature (K) = | 1974 |
| Particle Boiling Temperature (K) = | 1594 |
| Inlet Gas Velocity (m/s) = | 29.3 |
| Inlet Particle Velocity (m/s) = | 25 |
| Bulk Seed Mass Fraction (%) = | 1 |
| Overall Stoichiometric Ratio = | 1.0 |
| Inlet Fuel Concentration = | 0.368 |
| Inlet Inert Concentration = | 0.390 |
| Inlet Product Concentration = | 0.242 |
| Jet Mass Flow Rate (kg/s) = | 0.454 |
| Jet Temperature (K) = | 300 |
| Jet Oxidizer Concentration = | 1.0 |

Multiphase flow patterns for various oxidizer jet angles were computed and compared. Oxidizer jet angle was found to have a great effect on combustion performance as well as particle evaporation. Predicted flow patterns of a co-flow injection (jet angle smaller than 90 degrees) case contrast sharply with those of counter-flow injection (jet angle larger than 90 degrees). For co-flow injection the oxidizer jets do not penetrate significantly into the main flow, but rather are rapidly turned into the downstream forming a thick high gradient region near the walls. This flow configuration creates a nearly pure diffusion flame with a relatively low rate of mixing and combustion compared to the counter-flow degree injection case. The change of flow patterns greatly affects the combustion performance, especially, the uniformity of temperature profile at the exit plane, which has great influence on the seed particle vaporization and vapor dispersion. A large increase in combustion efficiency and particle vaporization occurs when going from co-flow injection to counter-flow injection. The angle for the highest combustion efficiency and the most effective particle vaporization and vapor dispersion is approximately 130 degrees.

Particle and gas flow patterns are significantly different in the vortex area as shown in Fig. 13. Velocity difference between gas and particles (or slip velocity) diminishes as particles move downstream in the combustor. The smaller the particle the smaller the slip velocity. For particles smaller than 5 μm, slip velocity is negligible and particle temperature reaches boiling temperature almost instantaneously. Some particles are trapped and deposited on the wall near the upstream edge of the oxidizer jet slots (Fig. 14a). Seed vapor is formed mainly in the central portion of the combustor and gradually diffused to the side walls as the gas flows downstream (Fig. 14b). Large particles (larger than 34 microns in diameter) can escape the combustor before complete vaporization (Fig. 15).

Design verification tests of the TRW's 50 MWt combustor were performed in the DOE's Component Development and Integration Facility (CDIF) in Butte Montana. Test results showed that (1) oxidizer injection angle is set at 135 degrees for maximum MHD performance, (2) growth of particle deposition was found in the second stage combustor, and (3) higher seed injection rate (70% more than design value) was required to achieve the design MHD performance (Braswell et al., 1993). The oxidizer injection angle agrees with the theoretical prediction in the previous discussion. The observed locations of particle deposition growth are in the predicted area as shown in Fig. 14a. The incomplete vaporization of the seed particles (Fig. 15) and the highly non-uniform seed vapor distributions (Fig. 14b) appears to lower the overall performance of the MHD power generation and results in a required higher seed injection rates used in the testing to boost MHD channel performance for the CDIF tests.

## 7. MASSIVELY PARALLEL MULTIGRID STRATEGY

In this section, we outline the strategy to solve the multiphase Navier-Stokes equations using massively parallel multigrid algorithms. Performance of the order of 2500 Mflops were reported for massively parallel computational fluid dynamics (CFD) single-phase multigrid algorithms using a SUPRENUM type of architecture with a successive over relaxation (SOR) Gauss-Seidel smoother (Alef, 1991). Tests of the parallel multigrid versions of the algorithm will be performed on Argonne National Laboratory IBM SP-1 parallel computer facility to test the performance of the proposed algorithms. The Fortran parallel language used in this work will be the portable parallel virtual machine (PVM) (Beguelin et al., 1991), and the P4 (Butler and Lush, 1992). These two languages are very similar and are chosen because most software developers use either or both language. Let us first review the basic principles involved in multigrid techniques and then the parallel computing techniques.

### 7.1. The Multigrid Concept

The concept of the multigrid technique can be explained as follows. Consider a set of linear finite-difference equations,

$$L^M W^M = F^M \tag{18}$$

for a general elliptic operator $L$, where $W$ is the solution vector. Any iterative procedure such as Gauss-Seidel or Jacobi converges rapidly for the first few iterations and very slowly thereafter. A Fourier analysis of the error-reduction process shows that these conventional iterative procedures are most efficient in smoothing out errors of wavelengths comparable to the mesh size, but are inefficient in annihilating low-frequency components. The multigrid technique is based on the premise that each frequency range of error must be smoothed on the grid where it is most suitable to do so. Consequently, the multigrid technique cycles between coarse and fine grids until all frequency components are appropriately smoothed.

The multigrid method cycles between a hierarchy of computational grids $D^k$ with corresponding functions $W^k$, $k = 1, 2, ..., M$. The step size on $D^k$ is $h_k$ and $h_{k+1} = 1/2h_k$, so that as $k$ decreases, $D^k$ becomes coarser. By doubling the mesh size in each direction (see Fig. 16, which shows the full coarsening technique) several levels of coarse grids are generated. In the full approximation storage (FAS) procedure (Brandt, 1984), the solution is initialized on the finest grid $M$. When the relaxation procedure (iteration) fails to smooth the residuals at the desired theoretical rate on the finest grid M, the iterations are stopped on grid $M$ and the residuals ($F^M - L^M w^M = R^M$; $w^M$ is an approximation to $W^M$) are transferred to the next coarser grid (restriction). On the coarser grid $D^{k-1}$, the equation solved is

$$L^{k-1} w^{k-1} = F^{k-1} + I_k^{k-1}\left(F^k - L^k w^k\right) - R^{k-1} \tag{19}$$

where $L^{k-1}$ is the operator on grid $D^{k-1}$, and $I_k^{k-1}$ is the operator to restrict (project) the $k$ variables on grid $k-1$, $R^{k-1}$ is restricted to grid $k-2$ and a solution of Eq. 19 is sought on grid $k-2$. When an accurate solution of Eq. 19 is obtained, the change from the previous value $w^{k-1} - I_k^{k-1} w_{old}^k$ is prolongated (bilinear interpolation) to grid $k$. The correction to $w^k$ is then

$$w_{new}^k = w_{old}^k + I_{k-1}^k\left(w^{k-1} - I_k^{k-1} w_{old}^k\right) \tag{20}$$

The iterations on each grid $k$ are continued until the required convergence criterion $|e^k| \leq \varepsilon^k$ is met, at which time the solution vector is transferred to the next finer level ($e^k$ is the tolerance level allowed on grid $k$). When the finest level is solved to the desired accuracy, the overall solution cycle is terminated.

Such multigrid algorithms have been successively used by Vanka (1986) and Bouillard and Berry (1992) in the solution of Navier-Stokes equations for single-phase fluid flows on serial machines. Essentially, the technique consists in solving the momentum equations and adjusting the pressures and velocities to satisfy the continuity equations. The multigrid version of the single-phase algorithm was recently extended by Thompson et al. (1992) for parallel shared-memory computers. A nearly linear speed-up scaling relationship was achieved as the number of processors was increased. Similar work has also been performed by Alef (1991). The proposed multigrid strategy would consist in adopting the prolongations and restrictions of Eqs. 19 and 20 to the fluid continuity equation residuals of the two-phase Navier-Stokes equation solver discussed above.

### 7.2. The Parallel Multigrid Strategy

In a parallel algorithm, the total number of computational cells is decomposed into patches that are assigned to each computer. This is represented in Fig. 17. In a shared-memory architecture, all the computational cells reside in a common memory. It is important that common data not be updated by two processors at the same time. To avoid this conflict, special software systems called monitors have been created. The monitor guarantees that the initialization is performed before contention for the share data begins and that only one of the operations may be performed at only one time. For detailed presentation on monitors (see Boyle et al., 1987). Such a principle was recently used by Thompson et al. (1992) to solve a multigrid single-phase flow problem on a small number of processors (15-20). Speed-up factors of the order of 15 were achieved on a moderate number of processors (20 processors on the Sequent Symmetry). This leads us to conclude that about one order of magnitude speed-up could be gained by using multigrid techniques and another order of magnitude could be gained using a moderate number of processors. This could result in two orders of magnitude speed-up and gigaflop performance using only a moderate number of processors. To avoid data dependencies between the processors, a Jacobi smoother will be used in the multigrid technique. Since the use of the parallel programming language (PVM and P4) proposed in this project is transportable to distributed-memory parallel processors, the same FORTRAN code could easily be extended to be used on the distributed massively parallel processors such as the Intel touchtone delta.

## 8. CONCLUSIONS

Applications of FLUFIX as incorporated into FORCE2 in atmospheric gas-solids fluidized beds have been successfully carried out, as demonstrated in this paper. Favorable comparisons with data have been shown and indicate that the models and modeling approach are sound. Many features, such as three dimensions, variable control volume size, flow resistance coefficients, and volume porosities and surface permeabilities, needed to model industrial-scale fluidized beds, have been implemented in FORCE2. With our three-dimensional hydrodynamic computer code FORCE2, it is now possible to better model complex large-scale fluid-solids systems, including atmospheric and pressurized bubbling and circulating fluidized bed combustors gasifiers and incinerators, and slurries for many industrial applications.

The integral reacting flow (IRF) computer code was used to simulate multiphase reacting flow in a TRW 50 MWt MHD second stage combustor. The simulation predicts the effects of combustor operation parameters on combustion efficiency, particle wall deposition, seed particle evaporation, and vapor dispersion characteristics in the combustor, which are crucially important to the performance of the overall MHD power generation. The predictions are in good agreement with test results.

An advanced multigrid, multiphase Navier-Stokes equation solver strategy for using massively parallel computer architectures is proposed on distributed multi-instruction multi-data (MIMD) shared-memory.

Such parallel multigrid computer programs do not presently exist and the development of such numerical solver would help bridge this gap. The use of the proposed massively parallel multigrid strategies could help reduce the excessive computer running time, typically from hours or days to few minutes, and thus bring routine design calculations of fluid-solids hardware in the practical realm of the engineer or the scientist.

## ACKNOWLEDGMENT

This study was supported under the Cooperative R&D Venture "Erosion of FBC Heat Transfer Tubes," Contract W-31-109-ENG-38. Members are the U.S. Department of Energy Morgantown Energy Technology Center; Electric Power Research Institute; State of Illinois Center for Research on Sulfur in Coal; Foster Wheeler Development Corp.; ASEA Babcock PFBC; ABB Combustion Engineering, Inc.; Tennessee Valley Authority; British Coal Corporation; CISE Tecnologie Innovative; and Argonne National Laboratory.

This work was also supported by U.S. Department of Energy, Assistant Secretary for Fossil Energy, under Contract W-31-109-ENG-38. Information provided by TRW, Inc. is greatly appreciated.

## REFERENCES

Alef, M., 1991, "Concepts for Efficient Multigrid Implementation on Suprenum-like Architectures," *Parallel Computing*, **17**: pp. 1-16.

Beguelin, A., Dongarra, J., Manchek, R., and Sunderam, V., 1991, "A User's Guide to PVM Parallel Virtual Machine," Oak Ridge National Laboratory Report ORNL/TM-11826, Oak Ridge, TN.

Bouillard, J.X., Lyczkowski, R.W., and Gidaspow, D., 1989, "Porosity Distributions in a Fluidized Bed With an Immersed Obstacle," *AIChE Journal*, **35**, pp. 908-922.

Bouillard, J.X., and Berry, G.F., 1992, "Performance of a Multi-Grid-Three-Dimensional MHD Generator Calculation Procedure," *International Journal of Heat and Mass Transfer*, **35**(9): pp. 2219-2332.

Boyle, J., Butler, R., Disz, T., and Glickfeld, B., 1987, *Portable Programs for Parallel Processors*, Holt, Rinehart and Winston Inc., NY.

Brandt, A., 1984, "Multigrid Techniques: Guide with Applications to Fluid Dynamics," Von Karman Institute, Lecture Series.

Braswell, R., Koyama, T., McAllister, M., Myrick, S., and Pote, B., 1993, "50 MWt Prototypical Combustor Performance," *Proceedings of 31st Symposium of Engineering Aspects of Magnetohydrodynamics*, Whitefish, MT, pp. II.1.1-17.

Burge, S.W., 1991, "FORCE2: A Multidimensional Flow Program for Gas-Solids Flow Theory Guide and User's Guide," Babcock & Wilcox Company, Research & Development Division Report, RDD:4911-10-01/02, Alliance, Ohio. Reprinted as DOE/MC/24193-3503/4.

Butler, R., and Lusk, E., "User's Guide to the P4 Programming System," Argonne National Laboratory Report ANL-92/17, Argonne, IL.

Chang, S.L., and Wang, C.S., 1987, "Thermal Radiation and Spray Group Combustion in Diesel Engines," ASME Winter Annual Meeting, Boston, MA, HTD-81:25-34.

Chang, S.L. and Lottes, S.A., 1993, "Integral Combustion Simulation of a Turbulent Reacting Flow in a Channel with Cross-Stream Injection," *Numerical Heat Transfer Part A*, **24**(1), pp. 25-43.

Chang, S.L., Lottes, S.A., Bouillard, J.X., and Petrick M., 1993, "Study of Multi-Phase Flow Characteristics in an MHD Power Train," *Proceedings of 31st Symposium of Engineering Aspects of MHD*, Whitefish, MT, pp. Vb.2.1-12.

Davidson, J.F., 1961, "Symposium on Fluidization - Discussion," *Transactions of the Institution of the Chemical Engineers*, **39**, pp. 230-232.

Ding, J., and Lyczkowski, R.W., 1992, "Three-Dimensional Kinetic Theory Modeling of Hydrodynamics and Erosion in Fluidized Beds," *Powder Technology*, **73**(2), pp. 127-138.

Ergun, S., 1952, "Fluid Flow through Packed Columns," *Chem. Eng. Prog.*, **48**, pp. 89-94.

Gidaspow, D., 1986, "Hydrodynamics of Fluidization and Heat Transfer: Supercomputer Modeling," *Applied Mechanics Reviews*, **39**(1), pp. 1-23.

Gidaspow, D., and Ding, J., 1990, "Predictive Models for Circulating Fluidized Bed Combustors: Three-Dimensional Code," DOE Report, DOE/PC/89769-1, (NTIS no. DE90010842).

Gidaspow, D., and Syamlal, M., 1985, "Solids-Gas Flow," presented at *AIChE 1985 Annual Meeting*, Chicago, IL, Nov. 10-15, 1985, paper no. 74e.

Harlow, F.H., and Amsden, A.A., 1975, "Numerical Calculation of Multiphase Fluid Flow," *Journal Computational Physics*, **17**, pp. 19-52.

Lottes, S.A., and Chang, S.L., 1992, "Particle-Jet Interactions in an MHD Second Stage Combustor," *Proceedings of 30th Symposium of Engineering Aspects of MHD*, Baltimore, MD, pp. VI.4.1-12.

Lyczkowski, R.W., Bouillard, J.X., Gidaspow, D., and Berry, G.F., 1990, "Computer Modeling of Erosion in Fluidized Beds," Argonne National Laboratory Report, ANL/ESD/TM-1, Argonne, IL.

Lyczkowski, R.W., Bouillard, J.X., Folga, S.M., and Chang, S.L., 1992, "User's Manual for EROSION/MOD1: A Computer Program for Fluid-Solids Erosion," Argonne National Laboratory Report, Argonne, IL. Reprinted as DOE/MC/24193-3500.

Lyczkowski, R.W., and Bouillard, J.X., 1992, "Users Manual for FLUFIX/MOD2: A Computer Program for Fluid-Solids Hydrodynamics," Argonne National Laboratory Report, Argonne, IL. Reprinted as DOE/MC/24193-3501.

Lyczkowski, R.W., and Wang, C.S., 1992, "Hydrodynamic Modeling and Analysis of Two-Phase Non-Newtonian Coal/Water Slurries," *Powder Technology*, 69, pp. 285-294.

Patankar, S.W., 1980, *Numerical Heat Transfer and Fluid Flow*, Hemisphere Publishing, Washington, DC.

Podolski, W.F., Lyczkowski, R.W., Montrone, E., Drennen, J., Ai, Y.H., and Chao, B.T., 1991, "A Study of Parameters Influencing Metal Wastage in Fluidized Beds Combustors," *Proceedings of the 11th (1991) International Conference on Fluidized Bed Combustion*, E.J. Anthony, ed., American Society of Mechanical Engineers, Vol. 2, pp. 609-618.

Schnipke, B.J., 1986, "A Streamline Upwind Finite Element Method for Laminar and Turbulent Flow," Ph.D. Thesis, University of Virginia.

Smoot, L.D., 1984, "Modeling of Coal-Combustion Processes," *Progress, Energy and Combustion Science*, **10**, pp. 229-272.

Thompson, C.P., Cowell, W.R., and Leaf, G.K., 1992, "On the Parallelization of an Adaptive Multigrid Algorithm for a Class of Flow Problems," *Parallel Computing*, **18**, pp. 449-466.

Vanka, S.P., 1986, "Block-Implicit Multigrid Solution of Navier-Stokes Equations in Primitive Variables," *Journal Computational Physics*, **65**, pp. 138-158.

Wen, C.Y., and Yu, C.H., 1966, "Mechanics of Fluidization," *AIChE Symp. Ser.*, (ed. B.S. Lee), **62**, pp. 100-112, American Institute of Chemical Engineers, NY.

Zhou, X.Q., and Chiu, H., 1983, "Spray Group Combustion Processes in Air Breathing Propulsion Combustors," Paper AIAA-83-1323, AIAA/SAE/ASME, *19th Joint Propulsion Conference*, Seattle, WA.

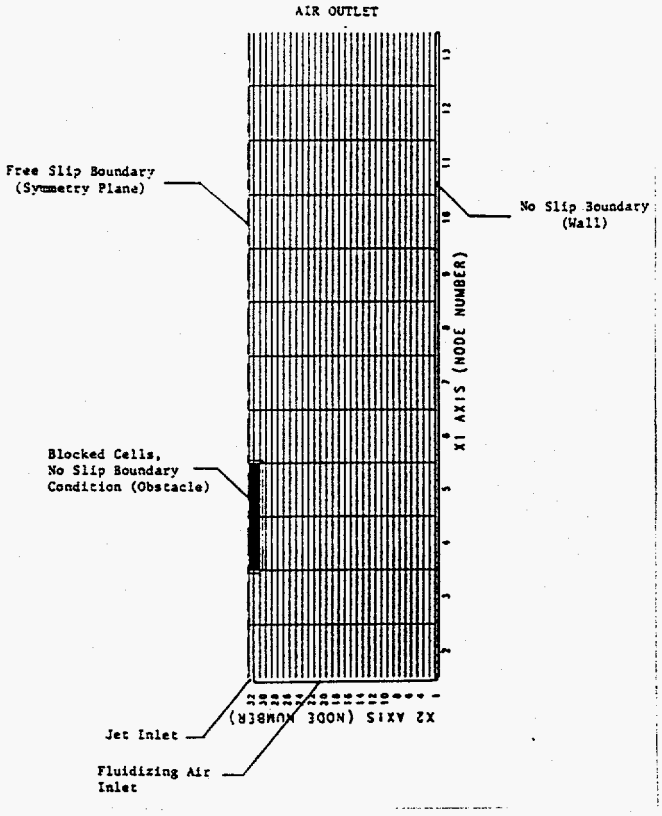


FIGURE 1. FORCE2 NODAL STRUCTURE USED FOR THE SOLUTION OF THE STANDARD PROBLEM

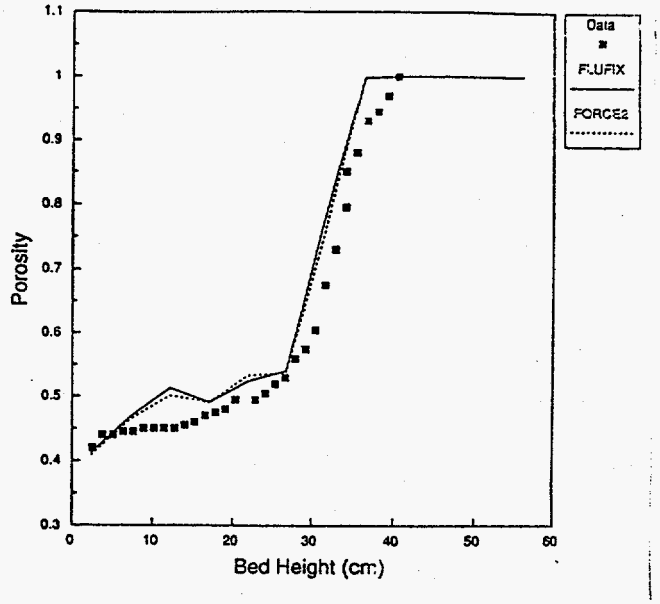


FIGURE 2. PREDICTED AND MEASURED TIME-AVERAGED BED POROSITIES 10 cm FROM THE CENTER OF THE JET, INVISCID SOLUTION ($\mu_S = 0$)

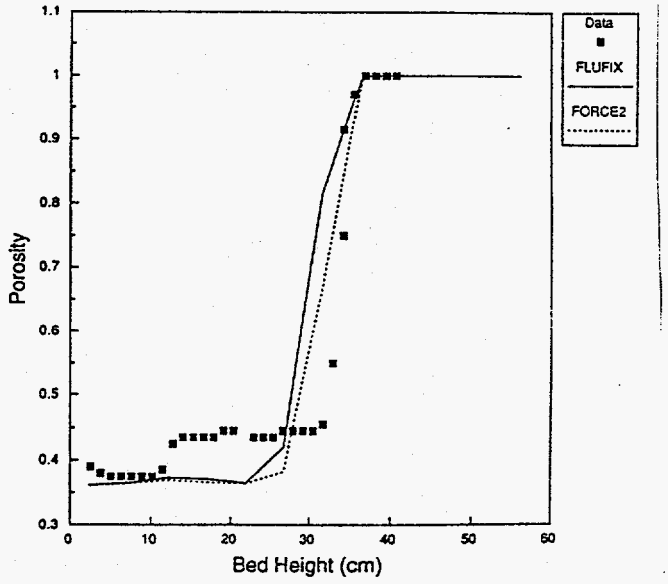


FIGURE 3. PREDICTED AND MEASURED TIME-AVERAGED BED POROSITIES 17 cm FROM THE CENTER OF THE JET, INVISCID SOLUTION ($\mu_S = 0$)

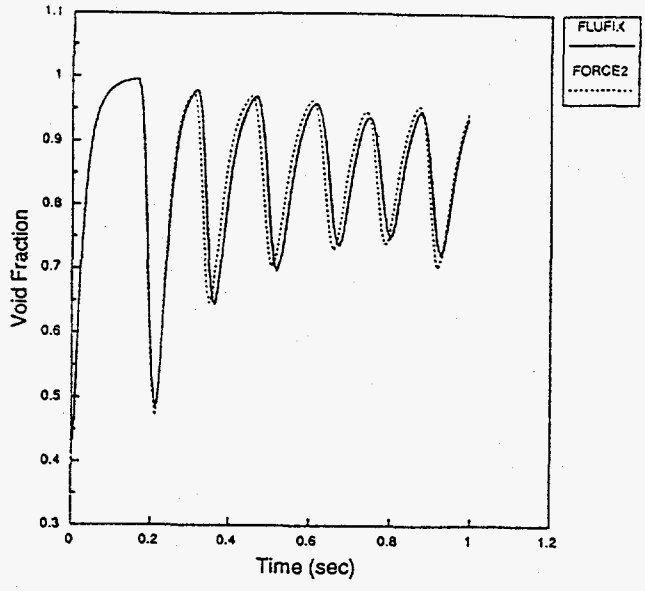


FIGURE 4. INSTANTANEOUS GAS VOID FRACTION PREDICTED BY FLUFIX AND FORCE2 IN THE NODE ABOVE THE JET, VISCOUS SOLUTION ($\mu_S = 0.1$ Pa·s)

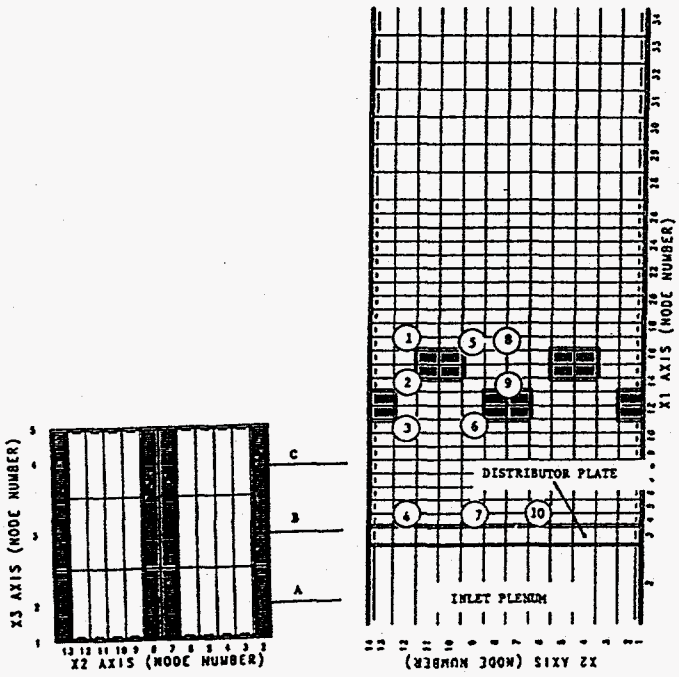


FIGURE 5. FORCE2 NODAL STRUCTURE USED TO MODEL THE 30.5 × 30.5-cm SQUARE FLUIDIZED-BED TUBE BUNDLE TESTED IN THE CAPTF

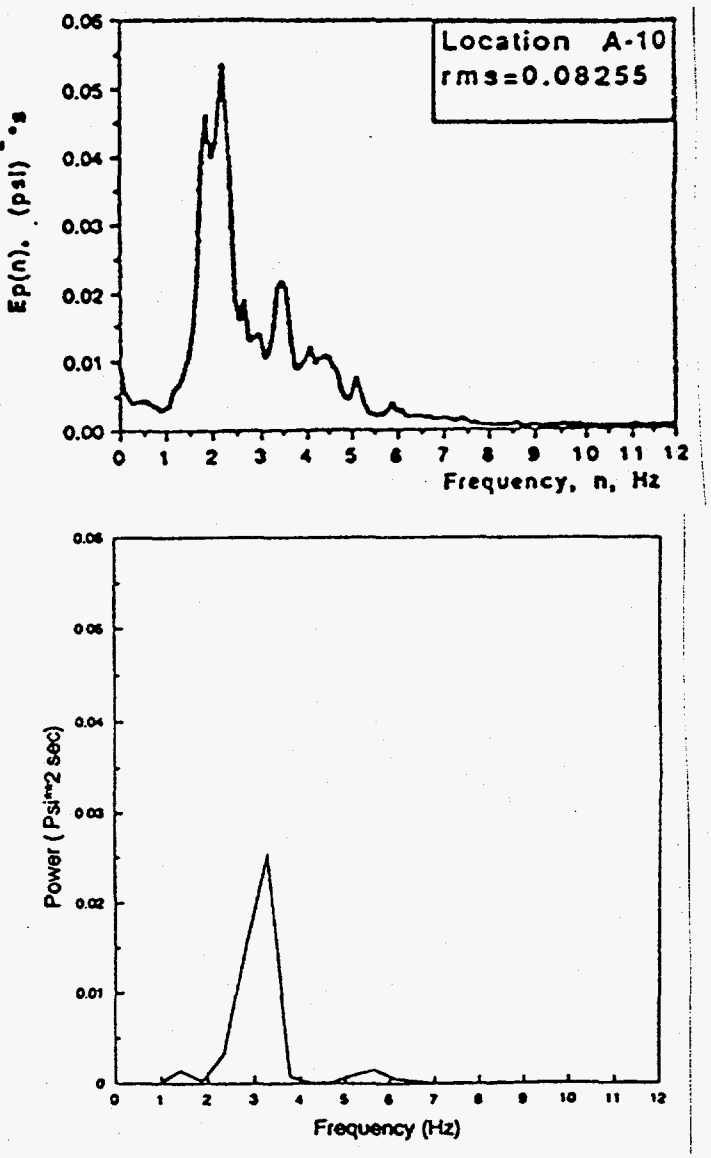


FIGURE 6. PREDICTED (LOWER) AND MEASURED (UPPER) POWER SPECTRAL DENSITIES OF THE PRESSURE FLUCTUATIONS IN THE 30.5 × 30.5-cm SQUARE CAPTF TUBE BUNDLE, LOCATION A-10

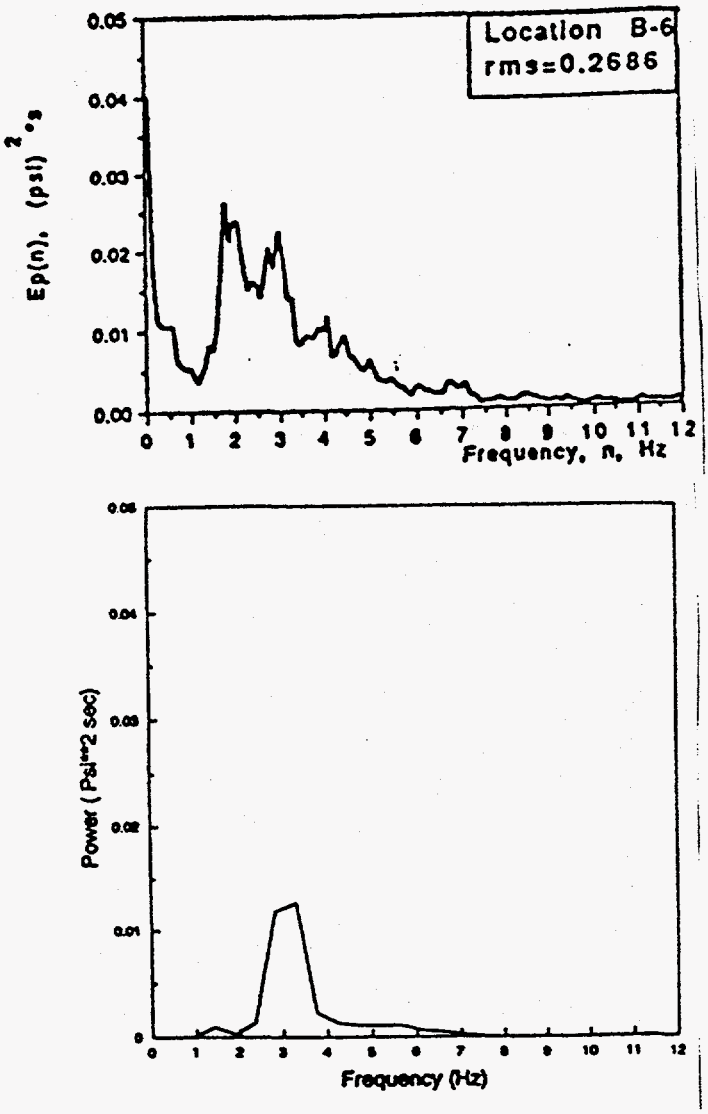


FIGURE 7. PREDICTED (LOWER) AND MEASURED (UPPER) POWER SPECTRAL DENSITIES OF THE PRESSURE FLUCTUATIONS IN THE 30.5 × 30.5-cm SQUARE CAPTF TUBE BUNDLE, LOCATION B-6

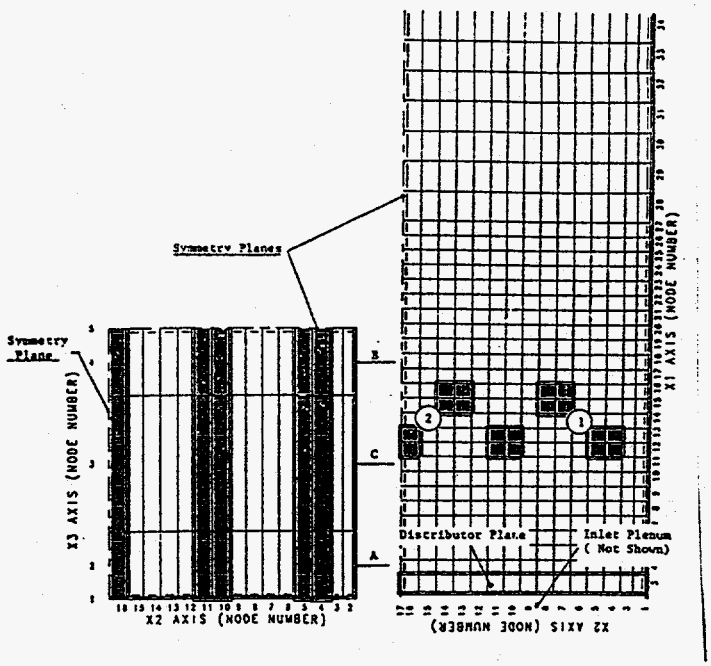


FIGURE 8. FORCE2 NODAL STRUCTURE USED TO MODEL THE FWDC HALF-DEPTH TUBE BUNDLE

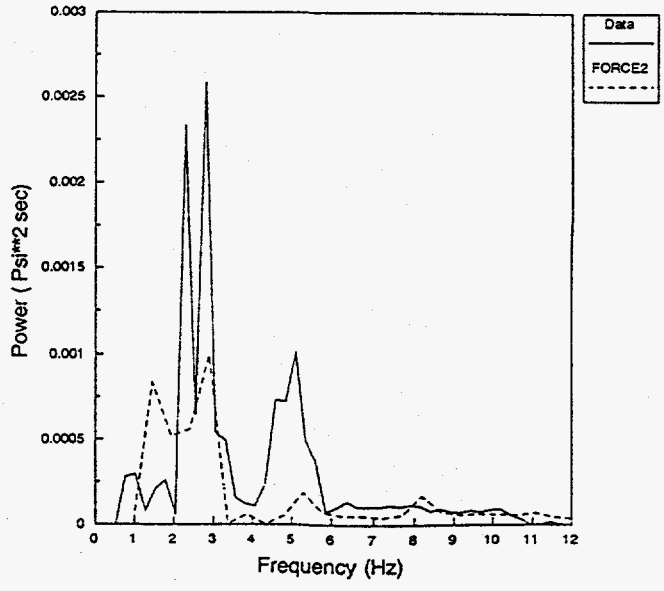


FIGURE 9. PREDICTED AND MEASURED POWER SPECTRAL DENSITIES OF THE PRESSURE FLUCTUATIONS IN THE FWDC HALF-DEPTH TUBE BUNDLE, LOCATION A-2

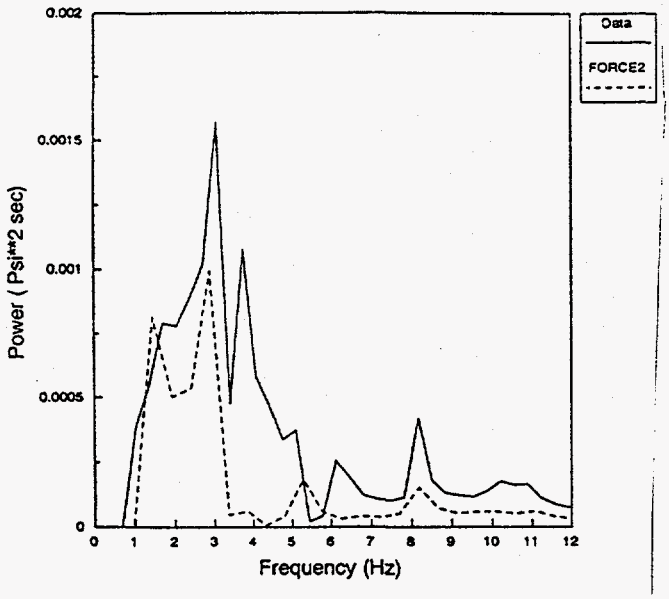


FIGURE 10. PREDICTED AND MEASURED POWER SPECTRAL DENSITIES OF THE PRESSURE FLUCTUATIONS IN THE FWDC HALF-DEPTH TUBE BUNDLE, LOCATION B-2

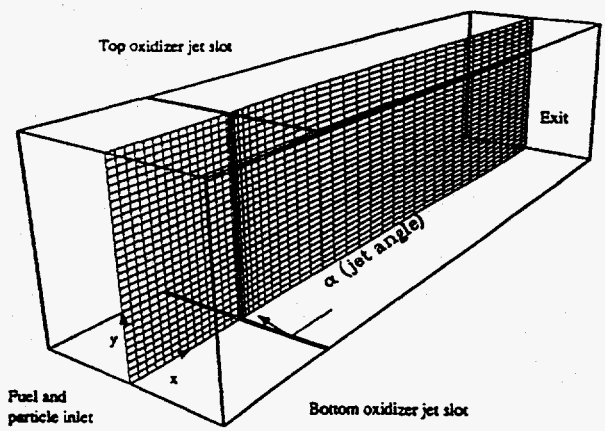


FIGURE 12. AN MHD COMBUSTOR AND A 54 BY 32 GRID

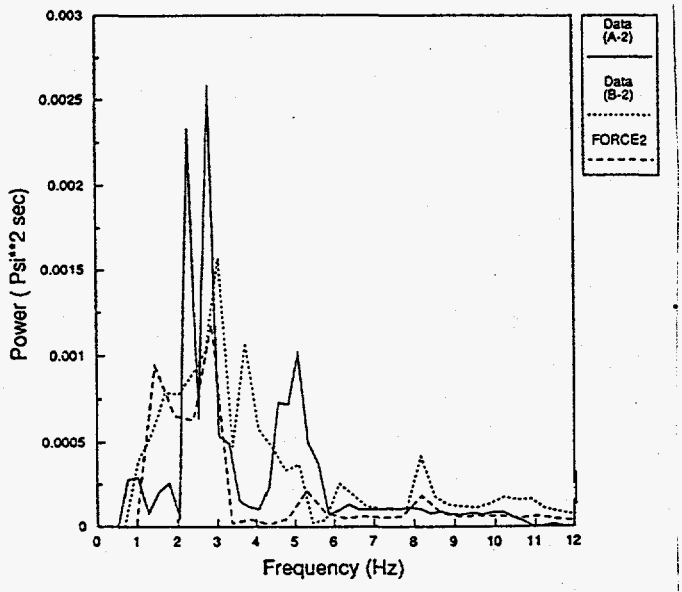


FIGURE 11. PREDICTED AND MEASURED POWER SPECTRAL DENSITIES OF THE PRESSURE FLUCTUATIONS IN THE FWDC HALF-DEPTH TUBE BUNDLE, LOCATIONS C-2 (PREDICTED) AND LOCATIONS A-2 AND B-2 (MEASURED)

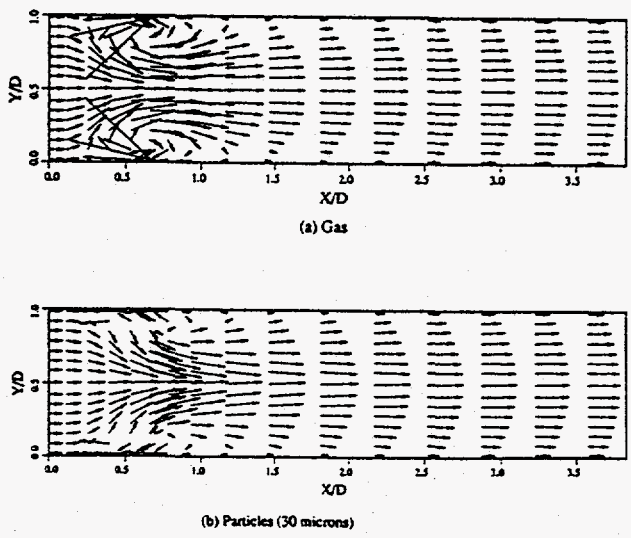


FIGURE 13. COMPARISON OF GAS AND PARTICLE FLOW PATTERNS

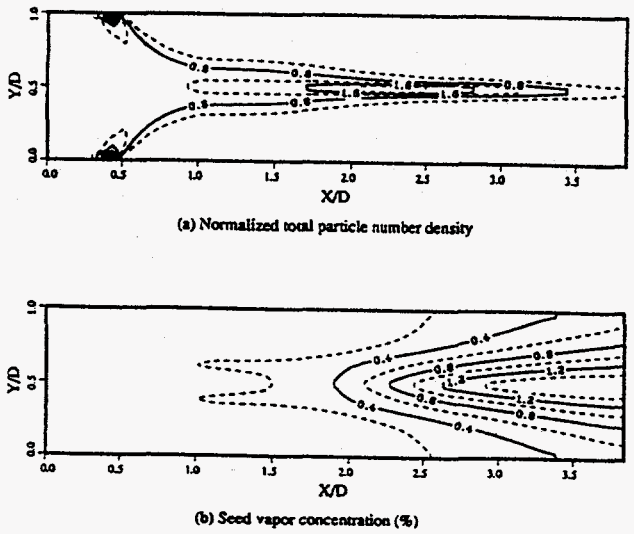


FIGURE 14. CHARACTERISTICS OF SEED PARTICLE EVAPORATION IN THE MHD COMBUSTOR

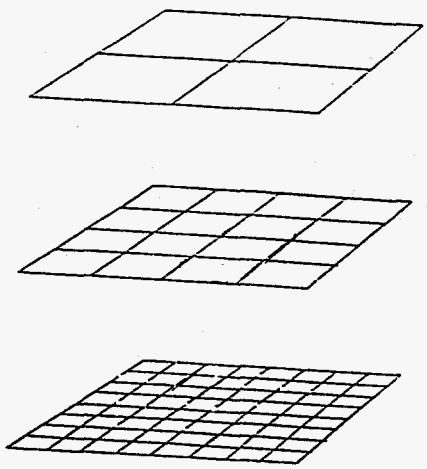

FIGURE 16. RELATIONSHIPS BETWEEN DIFFERENT MULTIGRID LEVELS

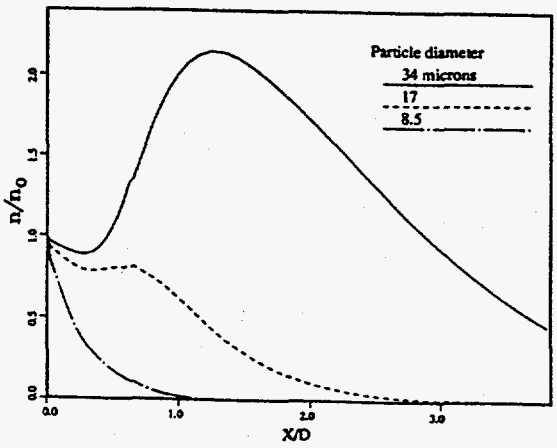


FIGURE 15. CENTERLINE PARTICLE NUMBER DENSITY IN THE MHD COMBUSTOR FOR VARIOUS SIZES

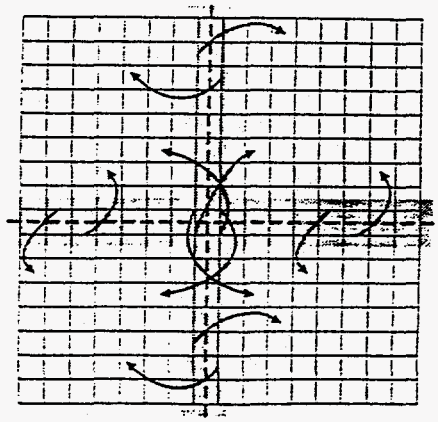

FIGURE 17. DOMAIN SPLITTING IN BOTH DIRECTIONS (TWO DIMENSIONS), EACH DOMAIN IS ASSIGNED TO A PROCESSOR